GFER#1499403, VOL 0, ISS 0

Strain-mediated all-magnetoelectric memory cell

V. Preobrazhensky, L. Krutyansky, N. Tiercelin, Y. Dusch, A. Sigov, P. Pernod, and S. Giordano

QUERY SHEET

This page lists questions we have about your paper. The numbers displayed at left can be found in the text of the paper for reference. In addition, please review your paper as a whole for correctness.

Q1. Please check whether the author names (first name followed by last name) and affiliations are correct as presented in the proofs.

TABLE OF CONTENTS LISTING

The table of contents for the journal will list your paper exactly as it appears below:

Strain-mediated all-magnetoelectric memory cell
V. Preobrazhensky, L. Krutyansky, N. Tiercelin, Y. Dusch, A. Sigov, P. Pernod, and S. Giordano

FERROELECTRICS
https://doi.org/10.1080/00150193.2018.1499403

Taylor & Francis
Taylor & Francis Group

Strain-mediated all-magnetoelectric memory cell

V. Preobrazhensky[a,b], L. Krutyansky[a,b], N. Tiercelin[b], Y. Dusch[b], A. Sigov[c], P. Pernod[b], and S. Giordano[b]

[a]Prokhorov General Physics Institute, RAS, Moscow, Russia; [b]University of Lille, CNRS, Centrale Lille, UMR 8520, IEMN, Lille, France; [c]Moscow Technological University (MIREA), Moscow, Russia

ABSTRACT

Downscaling of magnetoelectric random access memory device (MELRAM) is considered by studying an example of the hybrid structure based on ferroelectric-magnetostrictive metal. Elastic mechanism of magnetoelectric interaction is analyzed by numerical modeling taking into account inhomogeneous distribution of anisotropic strain, ferroelectric polarization and electric field. The proposed shape of the cell allows to decrease the inhomogeneity of the strain in the magnetic subsystem and to achieve remarkable dynamic characteristics for a nanometric device sized $50 \times 50 \times 400$ nm^3: we adopted an input voltage of $V_0 = 90$ mV and obtained a switching time $t_S = 1.1$ ns, an output readout voltage $V_{ME} = 4.7$ mV, and an ultra-low energy consumption 13 aJ/bit.

ARTICLE HISTORY
Received 27 April 2018
Accepted ▮▮▮

KEYWORDS
Ferroelectric; magnetoelectric memory; magnetostriction; inhomogeneous strain; dynamic parameters; energy efficiency

1. Introduction

Professor Petzelt has brought a valuable contribution to the area of ferroelectrics and related materials as well as to experimental methods of their properties investigation [1–3]. Nowadays, the family of ferroelectric materials is extended to hybrid nanostructures containing magneto-ordered components in addition to ferroelectric materials [4–8]. Such a kind of structures, known as composite or artificial multiferroics, is of interest for various applications due to a strong coupling between electric and magnetic subsystems mediated by the elastic strain. In particular, the strain-mediated magnetoelectric interaction is one of the most prospective principles of random access memory that ensures ultra-low energy consumption of the devices [9–11]. This principle allows writing information in the magnetic subsystem as well as detecting the magnetic states by means of electric field pulses [12,13]. The design of the magnetoelectric memory (MELRAM) requires a detailed study of the strain-mediated interaction at the nanoscopic scale. In the present paper, we report the results of simulation for the strain distribution in the MELRAM nano-cell and of expected dynamic parameters of the device.

2. Magneto-electric interaction in the ferroelectric-magnetic nanostructure

As a basic constituent of the cell, we consider a ferroelectric nano-pillar ($200 \times 75 \times 500$ nm^3) shaped on the crystal substrate PMN-PT <011> (see Figure 1a).

CONTACT A. Sigov assigov@yandex.ru
Joint International Laboratory LIA LICS
Color versions of one or more of the figures in the article can be found online at www.tandfonline.com/gfer.

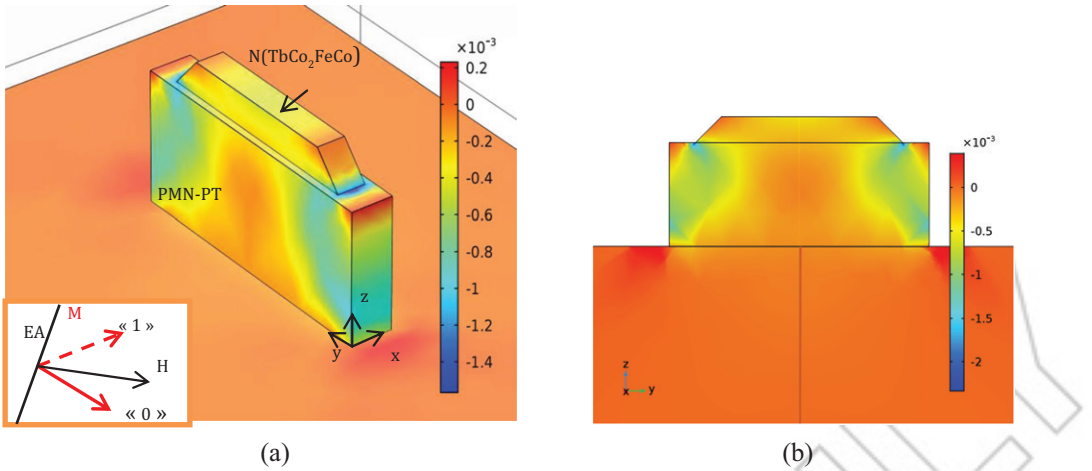

Figure 1. Strain distributions: (a) on the surface of the MELRAM cell; (b) over the section $x = 0$. The inset shows orientations of the easy axis (EA), magnetizing field ***H***, and magnetic moment ***M*** in both stable states.

The specific symmetry of the crystal provides a strongly anisotropic piezoelectric stress in the plane normal to the dielectric polarization and to the applied electric field. As a magnetic component, we propose an intermetallic multilayer with giant magnetostriction $N^*(TbCo_2/FeCo)$ $(50 \times 50 \times 400\,nm^3)$, deposited on the pillar. The anisotropy of the piezoelectric stress is a necessary condition for elastic coupling of ferroelectric and magnetic subsystems via magnetostriction [14]. The intermetallic multilayer acts also as the top electrode. On the other hand, the bottom electrode is located on the substrate around the pillar. The principle of MELRAM assumes the bistability of the magnetic subsystem and the switch of the magnetic moment from one stable state to another is performed by an electric pulse tension applied to the electrodes. The bistability is created by uniaxial magnetic anisotropy induced in the multilayer during the deposition process and by the application of a static magnetic field of suitable value and orientation, as discussed below. Equilibrium orientations of magnetization in the film are shown on the inset in Figure 1a (see the arrows labeled "0" and "1"). At the nanoscopic scale the elastic and electrodynamic boundary conditions affect essentially the parameters of devices. The shape of the cell presented in Figure 1 is chosen to reduce as much as possible the inhomogeneity of the strain distribution induced in the magnetic subsystem by the piezoelectric stress. The numerically simulated strain distribution on the surfaces of the pillar and magnetic film is shown in Figure 1a by a color map. The slice presented in Figure 1b illustrates the correspondent strain distribution in the volume of the cell.

The strain is generated by application of the voltage $V_c = 0.2$ V between the electrodes. The calculation was made by means of the COMSOL Multiphysics software using the set of elastic, piezoelectric and electric parameters for PMN-PT <011> crystal given, for instance, in [15]. The Young modulus of the magnetic film was assumed equal to 126 GPa, its density was 9.6×10^3 kg/m^3, and the Poisson's ratio was 0.345.

The value of the anisotropic part of the strain tensor, averaged over the volume of the film, was found as large as $<u_{xx} - u_{yy}> = -3.26 \times 10^{-4}$. The magnetoelectric

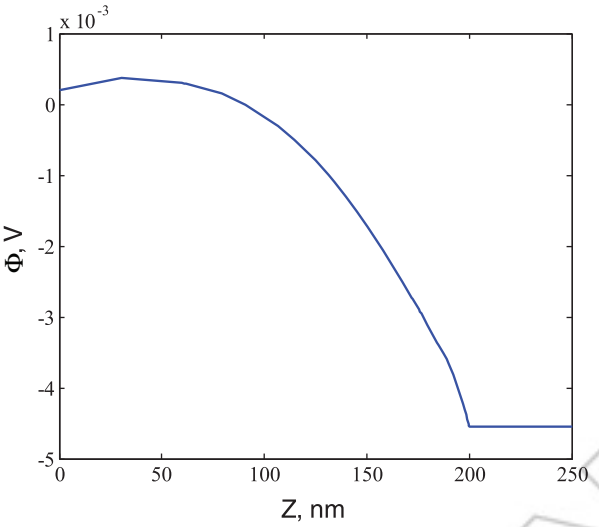

Figure 2. Electric potential induced by the magnetostrictive stress versus distance from the bottom of the ferroelectric pillar and the top of the magnetic layer. A zero potential is assumed on the electrode surrounding the bottom of the pillar.

coupling factor of the cell defined as $\alpha_{ME} = <u_{xx} - u_{yy}>/V_c$ appeared to be $\alpha_{ME} = -1.63 \times 10^{-3}$ V^{-1}. The anisotropic strain in the magnetic film is responsible for the control and the switching of the magnetic moment between stable states "0" and "1" via electric field. The polarity of the electric field defines the magnetic state after application of the electric pulse for writing information.

On the other hand, the magnetic moment switching generates an elastic stress in the ferroelectric pillar. The magnetically induced elastic stress is accompanied by the variation of ferroelectric polarization and by the generation of the electric pulse V_{MS} between the electrodes. This mechanism is used for magnetoelectric readout of information [12]. The initial magnetic state is identified by the reaction of the ferroelectric subsystem on the readout electric pulse of a fixed polarity. The response tension V_{MS} appears only if polarity of the readout pulse provides switching of magnetization from the initial state. Figure 2 shows the distribution of the electric potential generated in the pillar by the elastic stress $\sigma_{xx} - \sigma_{yy}$ homogeneously induced in the magnetic film when the magnetic moment switches from "0" to "1" or from "1" to "0". The factor of transformation of magnetostrictive stress to electric voltage on the cell defined as $\beta_{MS} = V_{MS}/(\sigma_{xx} - \sigma_{yy})$ is found equal to $\beta_{MS} = -4.56\ 10^{-4}$ V/MPa. Moreover, the calculated electric capacitance of the cell is equal to $C = 1.57$ fF.

3. Dynamic model of the MELRAM cell

The magnetic energy density F_m of the magnetic subsystem consists of Zeeman energy related to the magnetic moment $\boldsymbol{M}$ interacting with the magnetic field $\boldsymbol{H}$, the energy of the uniaxial magnetic anisotropy, and, finally, the demagnetizing energy

$$F_m = -\vec{M}\vec{H} - \frac{H_A}{2M}(\vec{M}\vec{n}) - \frac{1}{2}\vec{M}\vec{H}^m, \quad (1)$$

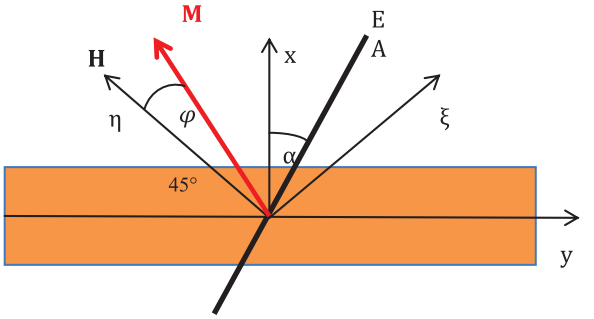

Figure 3. Geometry of the magnetic subsystem.

where $\boldsymbol{n}$ is the direction of the easy axis of magnetization, H_A and H^m are anisotropy and demagnetizing field, respectively.

The geometry of the magnetic subsystem is shown in Figure 3.

The energy of isotropic magnetoelastic interaction is represented as

$$F_{me} = \frac{B}{M^2} M_i M_j u_{ij}, \tag{2}$$

where B is the magnetostriction constant.

The electric field applied to the ferroelectric pillar parallel or antiparallel to the z-axis generates in the plane of the magnetic subsystem a deformation $u_{xx} - u_{yy}$, which seeks to impose the magnetization in directions parallel to the x-axis or antiparallel to the y-axis (states "1" or "0"). In order to provide the stable states with equal energy for these two orientations, the values and directions of magnetizing, demagnetizing and anisotropy fields should be suitably chosen. As it is shown in Figure 3, the magnetizing field should be directed at 45° with respect to the ferroelectric crystalline axes. The angle α of the easy axis orientation depends on the ratio of demagnetizing and anisotropy fields. For the shape of magnetic structure presented in Figure 1, we assume a simplified model of a long magnetic bar with the following projections of the demagnetizing field: $H_x^m = -2\pi M_x$, $H_z^m = -2\pi M_z$, $H_y^m = 0$. In this case, the easy axis orientation is determined by the ratio $\cos 2\alpha = H^m / H_A$, where $H^m = 2\pi M$.

The magnetic energy in Eq. (1) has the following representation in the coordinate system associated with magnetizing field $\boldsymbol{H}$

$$F_m = -HM_\eta - \frac{H_A^{eff}}{4M}\left(M_\xi^2 - M_\eta^2\right) + \frac{\pi}{2}\left(1 + \frac{H_A}{H^m}\right)M_\zeta^2, \tag{3}$$

where the effective anisotropy field is: $H_A^{eff} = H_A\sqrt{1-(H^m/H^A)^2}$.

By considering the switch process of magnetic moment as a homogeneous rotation from one equilibrium position to another under piezoelectric stress, we substitute inhomogeneous deformation in Eq. (2) by its mean value averaged over the magnetic layer volume. Under this assumption, taking into account the definition of the magnetoelectric factor α_{ME} mentioned above, the magnetoelastic energy in Eq. (2) assumes the form

$$F_{me} = \frac{B}{M^2}\alpha_{ME} V_c(t) M_\xi M_\eta. \tag{4}$$

For the description of the MELRAM dynamics, we follow the approach developed in [13]. The magnetization switch under electric tension is described by the Landau–Lifshitz–Gilbert (LLG) equation

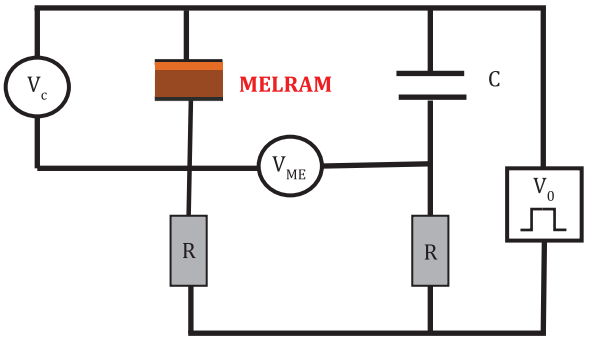

Figure 4. The electric scheme for magnetoelectric readout in the MELRAM cell. The magnetic state is identified by the pulse signal V_{ME} measured after application of a readout voltage pulse V_0.

$$\frac{\partial \vec{M}}{\partial t} = -\gamma \vec{T} + \frac{\delta}{M}\left[\vec{M} \times \frac{\partial \vec{M}}{\partial t}\right], \tag{5}$$

where γ is gyromagnetic ratio and δ is damping parameter. The torque vector $\boldsymbol{T}$ has the form

$$\vec{T} = -\left[\vec{M} \times \frac{\partial (F_m + F_{me})}{\partial \vec{M}}\right]. \tag{6}$$

For a better description of the nonlinear dynamics it is convenient to transform the LLG equation to the angular representation thus using the notations $M_\xi = M\cos\theta\sin\varphi$, $M_\eta = M\cos\theta\cos\varphi$, $M_\zeta = M\sin\theta$, where φ and ϑ are in-plane and out-of-plane magnetization angles, respectively. The LLG equation in the angular representation corresponds to the system of equations

$$\begin{aligned}\frac{\partial \varphi}{\partial t} &= -\frac{\gamma}{M\Delta}\left[T_\xi \cos\theta + T_\zeta(\sin\theta\sin\varphi - \delta\cos\varphi)\right]\\ \frac{\partial \theta}{\partial t} &= -\frac{\gamma}{M\Delta}\left[T_\xi \delta cos^2\theta + T_\zeta(\cos\theta\cos\varphi + \delta\sin\theta\cos\theta\sin\varphi)\right],\end{aligned} \tag{7}$$

where

$$\Delta = cos^2\theta\cos\varphi(1+\delta^2), \tag{8}$$

$$\begin{aligned}T_\xi/M &= \frac{1}{4}\left(H_A^{eff} - H_A - H^m\right)\sin 2\theta\cos\varphi - H\sin\theta + \frac{B}{2M}\alpha_{ME}V_c\sin 2\theta\sin\varphi\\ T_\zeta/M &= -\frac{1}{2}H_A^{eff}cos^2\theta\sin 2\varphi + H\cos\theta\sin\varphi + \frac{B}{M}\alpha_{ME}V_c cos^2\theta\cos 2\varphi.\end{aligned} \tag{9}$$

Since the magnetoelastic layer is mechanically coupled to the ferroelectric crystal, the dynamic reorientation of the magnetization described by Eq. (7) induces variations of the electric polarization in the ferroelectric subsystem.

Indeed, magnetically induced polarization contributes to the electric current J flowing through the cell is

$$J = C\frac{\partial}{\partial t}(V_c - V_{MP}), \tag{10}$$

where the magnetic contribution is expressed through the magnetoelectric tension

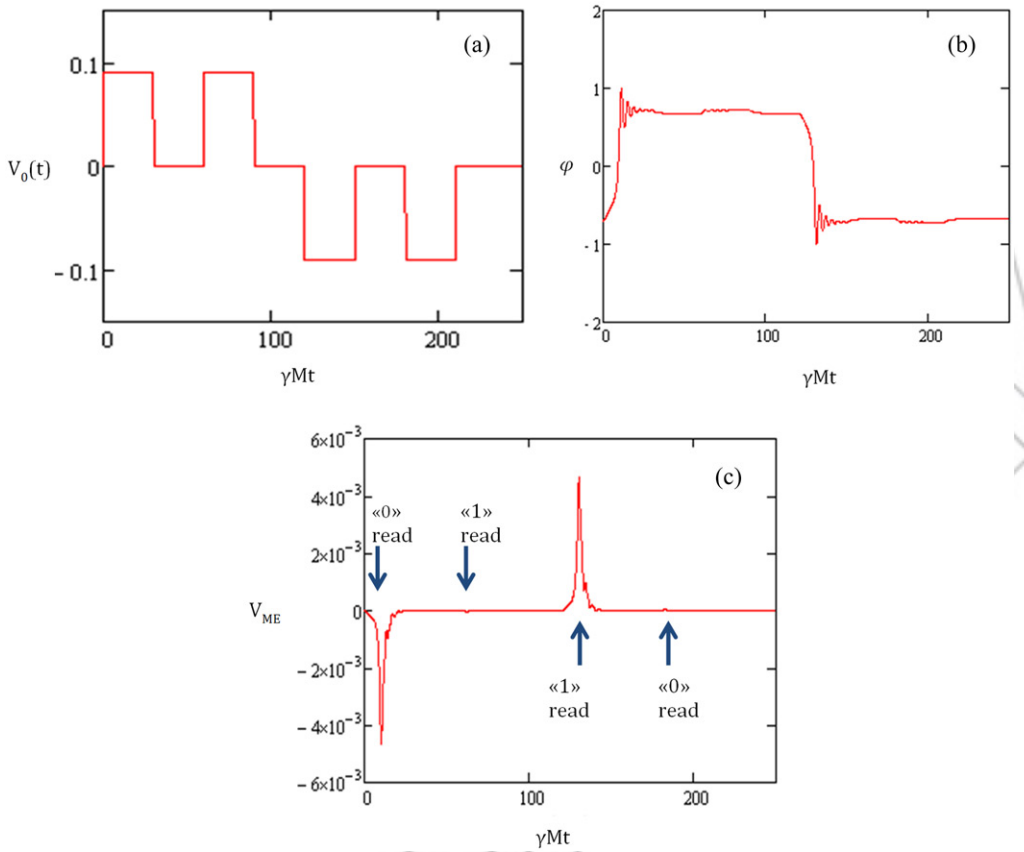

Figure 5. Reading and writing processes: (a) sequence of electric pulses used for the demonstration of the principle of magnetoelectric writing and readout in the MELRAM cell; (b) switch of the magnetization between equilibrium positions $\varphi = -\pi/4$ and $\varphi = \pi/4$; (c) magnetoelectrically induced readout pulses.

$$V_{MS} = 2\beta_{MS}\frac{B}{M^2}M_\xi M_\eta = \beta_{MS}B\sin 2\varphi. \tag{11}$$

Here we used definition of the factor β_{MP} introduced above.

For the description of both writing and reading processes of information, the LLG equation in the form of Eq. (7) should be completed by the electrodynamic equations for the electrical circuit in which the magnetoelectric cell is embedded. Following [13], we consider the simplest circuit constituted by a Wheatstone bridge, as shown in Figure 4. In this case, the V_c voltage on the structure and the magnetoelectric signal V_{ME} across the diagonal of the bridge are described by the equations

$$\begin{aligned} RC\frac{\partial V_c}{\partial t} + V_c - RC\frac{\partial V_{MS}}{\partial t} &= V_0(t) \\ RC\frac{\partial V_{ME}}{\partial t} + V_{ME} - RC\frac{\partial V_{MS}}{\partial t} &= 0, \end{aligned} \tag{12}$$

where R is the resistance of the bridge.

4. Results and discussion

The results of the numerical solution of the system composed by Equations (7) and (12) are presented in Figure 5. The following parameters of the system were assumed in the calculations: $M = 200$ emu/cm^3, H_A=1.3 kOe, $B = 10$ MPa, $RC = 0.6$ ns, $\delta = 0.1$. Writing and reading operations, performed by electric field application, are demonstrated by means of an example of a sequence of applied electric pulses, as presented in Figure 5a using the dimensionless time scale γMt with $\gamma M = 3.5\ 10^9$ s^{-1}.

The magnetic moment rotation from orientation $\varphi = -\pi/4$ (state "0") to orientation $\varphi = \pi/4$ (state "1"), under electric control, is shown in Figure 5b. The positive writing pulse $V_0 = 90$ mV generates a magnetization state "1". Application of the second positive pulse does not change the written state. To write the state "0", the electric pulse with negative polarity must be applied. Calculated switching time was found equal to $t_s = 1.1$ ns.

The written magnetic state can be identified by application of the readout electric pulse. For example, the first positive pulse of the sequence shown in Figure 5a generates a magnetic moment switch accompanied by the signal $V_{ME} = 4.7$ mV in the bridge diagonal (see Figure 5c). The appearance of the signal indicates the initial state "0". If necessary, this signal can be used also for triggering the inverse writing pulse for the restoration of the initial magnetic state. The absence of the signal V_{ME} after the second positive pulse indicates the initial state "1". Thus, the appearance or the absence of the V_{ME} signal after application of the readout pulse of given polarity indicates the initial state of the magnetic system. The calculated energy consumption for writing and reading operations was found equal to $E = 13$ aJ/bit. This value is close to the previously calculated one, based on the model of the effective magnetoelectric medium [13] and is much lower than $E = 6$ fJ/bit, recently obtained experimentally in a MTJ-RAM of comparable size [16]. The stability of the equilibrium magnetic states "0" and "1" over time is ensured by the energy barrier $E_b = (3 - 2\sqrt{2})\nu M H^{eff}/4$, where ν is the volume of the cell [11]. In the case under consideration, the long time stability of stored information at room temperature is defined by the parameter $E_b/k_BT = 73$.

In conclusion, we can affirm that in the downscaling process of the MELRAM device the mechanical and electrodynamic boundary conditions may significantly affect the dynamic parameters of the memory cells. Nevertheless the appropriate design of the cell allows achieving high speed and ultra-low energy consumption for the magnetoelectric writing and readout of information.

Funding

This work was supported by the RFBR grant 16-29-14022, and the PREMATURATION programs of the CNRS and I-Site ULNE (MELRAM project). The authors also wish to thank the French RENATECH network.

References

[1] J. Hlinka et al., Coexistence of the phonon and relaxation soft modes in the terahertz dielectric response of tetragonal $BaTiO_3$, *Phys. Rev. Lett.* **101** (16), 167402 (2008). [Database]

[2] J. Petzelt, Soft mode behavior in cubic and tetragonal $BaTiO_3$ crystals and ceramics: review on the results of dielectric spectroscopy, *Ferroelectrics* **375** (1), 156–164 (2008).
[3] J. Petzelt, and S. Kambra, Far infrared and terahertz spectroscopy of ferroelectric soft modes in thin films: a review, *Ferroelectrics* **503** (1), 19–44 (2016).
[4] C. W. Nan et al., Multiferroic magnetoelectric composites: historical perspective, status, and future directions, *J. Appl. Phys*. **103** (3), 031101–031135 (2008).
[5] N. Tiercelin et al., Thin film magnetoelectric composites near spin reorientation transition, *J. Magn. Magn. Mater*. **321** (11), 1803–1807 (2009).
[6] J. M. Hu, and C. W. Nan, Electric-field-induced magnetic easy-axis reorientation in ferromagnetic/ferroelectric layered heterostructures, *Phys. Rev. B* **80** (22), 224416-1–224416-11 (2009).
[7] J. L. Hockel *et al.*, Electric field induced magnetization rotation in patterned Ni ring/$Pb(Mg_{1/3}Nb_{2/3})0_3]_{(1-0.32)}$-$[PbTiO_3]_{0.32}$ heterostructures, *Appl. Phys. Lett*. **100** (2), 022401-1–022401-3 (2012).
[8] Z. Wang *et al.*, Electrical and thermal control of magnetic coercive field in ferromagnetic/ferroelectric heterostructures, *Phys. Rev. B* **89** (3), 035118-1–035118-5 (2014).
[9] J. M. Hu *et al.*, A simple bilayered magnetoelectric random access memory cell based on electric-field controllable domain structure, *J. Appl. Phys*. **108** (4), 043909-1–043909-6. (2010).
[10] N. Tiercelin *et al.*, Room temperature magnetoelectric memory cell using stress-mediated magnetoelastic switching in nanostructured multilayers, *Appl. Phys. Lett*. **99**, 192507 (2011).
[11] N. Tiercelin *et al.*, Strain mediated magnetoelectric memory, in *Nanomagnetic and Spintronic Devices for Energy Efficient Computing*, edited by S. Bandyopadhyay and J. Atulasimha (Wiley, New York, 2016), chapter 8, pp. 221–257, ISBN 978-1-118-86926-0.
[12] A. Klimov *et al.*, Magnetoelectric write and read operations in a stress-mediated multiferroic memory cell, *Appl. Phys. Lett*. **110** (22), 222401 (2017).
[13] V. Preobrazhensky *et al.*, Dynamics of the stress-mediated magnetoelectric memory cell N*($TbCo_2$/FeCo)/PMN-PT, *J. Magn. Magn. Mater*. **459**, 66–70 (2018).
[14] Y. Dusch *et al.*, Stress-mediated magnetoelectric memory effect with uni-axial $TbCo_2$/FeCo multilayer on 011-cut PMN-PT ferroelectric relaxor, *J. Appl. Phys*. **113** (17), 17C719.
[15] F. Wang *et al.*, Complete set of elastic, dielectric, and piezoelectric constants of orthorhombic $0.71Pb(Mg_{1/3}Nb_{2/3})0_3$-$0.29PbTiO_3$ single crystal, *Appl. Phys. Lett*. **90** (21), 212903 (2007).
[16] C. Grezes *et al.*, Ultra-low switching energy and scaling in electric-field-controlled nanoscale magnetic tunnel junctions with high resistance-area product, *Appl. Phys. Lett*. **108**, 012403 (2016).